The Effect of Fe Additive on Plastic Deformation for Crush-Boxes with Closed-Cell Metal Foams, Part I: Al-Composite Foam Compression Response

S.M.H.Mirbagheri [*] and J. Khajehali

Department of Mining and Metallurgical engneering, Amirkabir University of Technology, Tehran, Iran

Abstract: In this study, the effect of Fe–intermetallic compounds on plastic deformation of closed-cell composite Aluminum Foam as the filler of thin-walled tubes is investigated. Composite foams of AlSi7SiC3 and AlSi7SiC3-(Fe) as a closed cell were synthesized through powder metallurgy foaming method. Macro and Micro structures of the produced foams revealed a non-homogenous cell which is dependent on Fe-rich intermetallic compounds. The cellular structure of AlSi7SiC3 foam shows a non-uniform and small size of bubbles with a few central big voids in comparison with the AlSi7SiC3-(Fe) foams. The analysis of EDAX (Energy Dispersive Analysis of X-rays) indicate that there are $(\alpha+\beta)$-Fe- intermetallic compound within foams with Fe < 2 wt. %, and $(\alpha+\delta)$-Fe-intermetallic compound for the foams with Fe > 2 wt. %, in which their presence depend on the cooling rate during the solidification of liquid foams. The stress-strain curve of the AlSi7SiC3 foam shows a smooth plastic deformation behavior in the plastic region, throughout the compression tests. However, by increasing the weight percent of Fe from 1 up to 3%, the curve shows some variation at the slope of $Ln(\sigma) - Ln(\varepsilon)$ curves within the plastic zone. The results obtained indicated that all of the compression response is due to the micro-porosity in plateau region and the presence of the Fe-Al-Si-intermetallic within the cell wall revealed that both of them have the role of a stress concentration point during the compressive loading.

1. Introduction

In the last few decades, due to possessing unique combination of properties, Aluminum alloys foams have developed in variety of industries [1–3]. Metal foams as an advanced material are categorized into two groups based on their cellular structure, namely open cell foam, and closed cell foams. Industrial applications of the open cell foams are in the field of filtrations, thermal and ionic exchangers. However, the closed cell foams have an application of impact absorption, sound, and vibration energy, especially as a role of energy absorbers or the crash boxes in automobile industries. The closed cell metal foams can be manufactured through two main methods; casting and powder metallurgy [4-5]. With regard to the fabrication methods, Aluminum and Aluminum alloys are the best candidates for metallic foams due to their excellent mechanical and physical properties. Al-foams are considered as suitable materials for energy absorption due to their cellular structure. Al alloys foams demonstrate a distinctive plateau of almost constant stress in the uni-axial compressive stress-strain curve with the nominal strain value up to 75%, which indicates a high energy absorption capacity [3]. Regarding this issue, many research were done on mechanical properties and absorption energy of Aluminum foam, Al-the alloys foam, and Al composites foam as filler of thin-walled tubs. The quality of the Al composite foams has shown a significant influence on the pattern of the elastic and the plastic deformation of the foams and Al composite foam filled tubes [9-10]. The quality of the produced Aluminum composite foams is influenced by several parameters such as composition, particle distribution, volume fraction, size, shape, and matrix alloy composition, foaming temperature, holding time and cooling rate [11]. Several investigations

focused on compressive properties of the Al composite foams with reinforcing particles such as Al_2O_3 and SiC [12-14]. However, investigations on the effect of the elements with high melting point temperatures with respect to the matrix alloy melting point on the compressive properties are very few, especially when the combination of both the high melting point elements powder (such as Fe and Si) and the reinforcement particles are considered (as like SiC and TiB_2). Recently, it is reported that the compressive stress–strain curve of AlSi9Mg foams is smooth with hardening-strain, whereas AlSi9Mg–SiC composite foams are not smooth and exhibit some serrations, which often is associated with the hardening-strain [15]. Therefore, in the present investigation, the effect of Fe and SiC on micro-structural and behavior of plastic deformation for Al-Si foam as filler of crush-boxes, under the condition of quasi-static uni-axial compression load has been evaluated. Moreover, the mechanism of Fe powder addition on the elimination of strain hardening during plastic deformation has been described based on the creation of the ductile or brittle inter-metallic compounds and the micro-porosity into the Al-Si-SiC foam cellular structure

2. Experimental procedures

The present investigation makes use of powder mixtures such as Fe, Al-Si, SiC, and TiH_2 powders as a high melting point stabilizer, matrix alloy, reinforcement, and blowing agent for foam production process, respectively. Table (1) shows the characteristics of each powder. In order to assess the Fe additive on the cellular structure and the mechanical properties during plastic deformation, three types of composite foams namely AlSi7SiC3, AlSi7SiC3Fe1, and AlSi7SiC3Fe3 were designed and synthesized using powder metallurgy method. In order to produce the precursor, the powders mixture were then mixed with 1wt.% TiH_2 and, after cold iso-static was pressed into green cylinders with 63 mm diameter, it was hot extruded at 450 ◦C with the extrusion ratio of 63/14. Therefore, three types of precursors; AlSi7SiC3, AlSi7SiC3Fe1, and AlSi7SiC3Fe3 in each hot extrude will be prepared.

Table 1. Consume powders Characteristics

Chemical Composition	Purity (%)	Size (μm)
SiC	95	<25
TiH_2	98	<44
Si	95	<150
Fe	99	<44
Al	97	<63

The foaming treatment was carried out for all precursors in a resistance electrical furnace at 700 ◦C using several thin-walled tubs as mould. The tubular moulds with thickness of 1 mm, and outside diameters of 16, 22 and 35 mm were cut with the height of 1.5 times of their diameters, respectively. Then all the tubes were preheated to 700 ◦C. The obtained precursors from the hot extrusion were cut and put into the tubes separately and was held in the foaming temperature for 8-10 minutes, and immediately cooled through the forced air.

The uni-axial quasi static loading on the metal foams then were performed using 25 kN Instron 8502 test machine at a crosshead speed of 2.5 mm/min and 1.3×10^{-3} (1/sec) strain rate at room temperature for samples with 20mm diameter. The curve of stress-strain was plotted after that for the three foams. In

order to identify the Composite Metal Foam samples, they were coded as "CMF-Z-X-Y". Each code includes three parts: "Z", "X" and "Y". The letter "Z" refers to geometry of moulds (S=square, C=circle) and the letter "X" refers to diameter of foam cross-section as a millimeter (16 or 22, or 35mm), and "Y" indicates weight percent amount of the Fe powder in foams (Y= 0% or 1% or 3%).

However, in this part, all moulds had a circle cross-section. The "Z=C" in codes then were deleted and the obtained microstructures were investigated using an optical microscope and an X30 Philips scanning electron microscope was operated at 20 KV. Compositional spot analyses were performed at the interface of the inter-metallic compounds and the matrix alloy using an Energy Dispersive X-ray Analysis (EDXA) facility in the SEM.

3. Results and Discussions

3.1. Phases, compounds and cellular structure

Fig.1a. shows the distribution of the consumed powder particles based on Table (1) in the produced precursors.

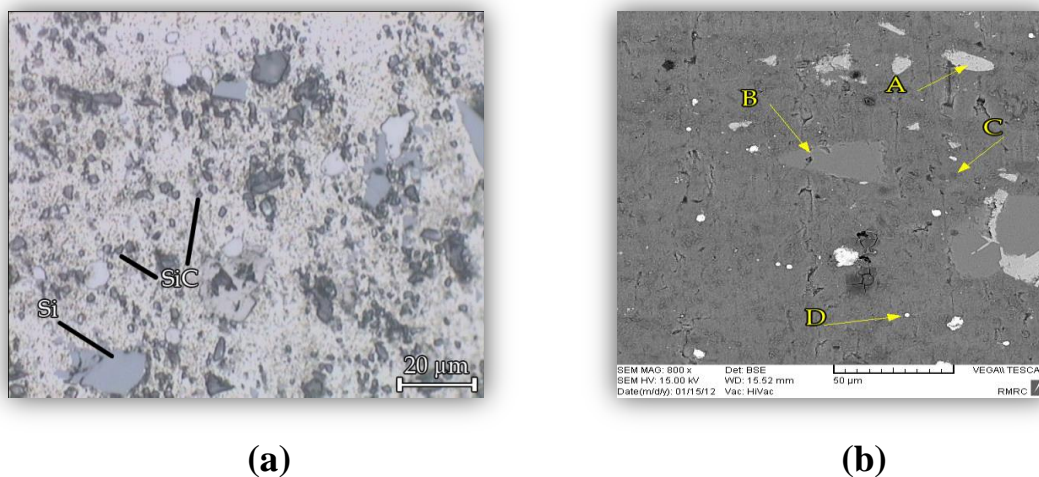**(a)**   **(b)**

Figure 1. Metallography of precursors and distribution of particles (types and sizes) in consumed powders; a) optical metallography, b) SEM metallography.

It is clear that the distribution of the particles is approximately homogenous in Fig.1b. The points shown in A, B, C, and D are selected in order to identify their composition by EDXA method. The obtained results from the EDXA are illustrated in Fig.2.
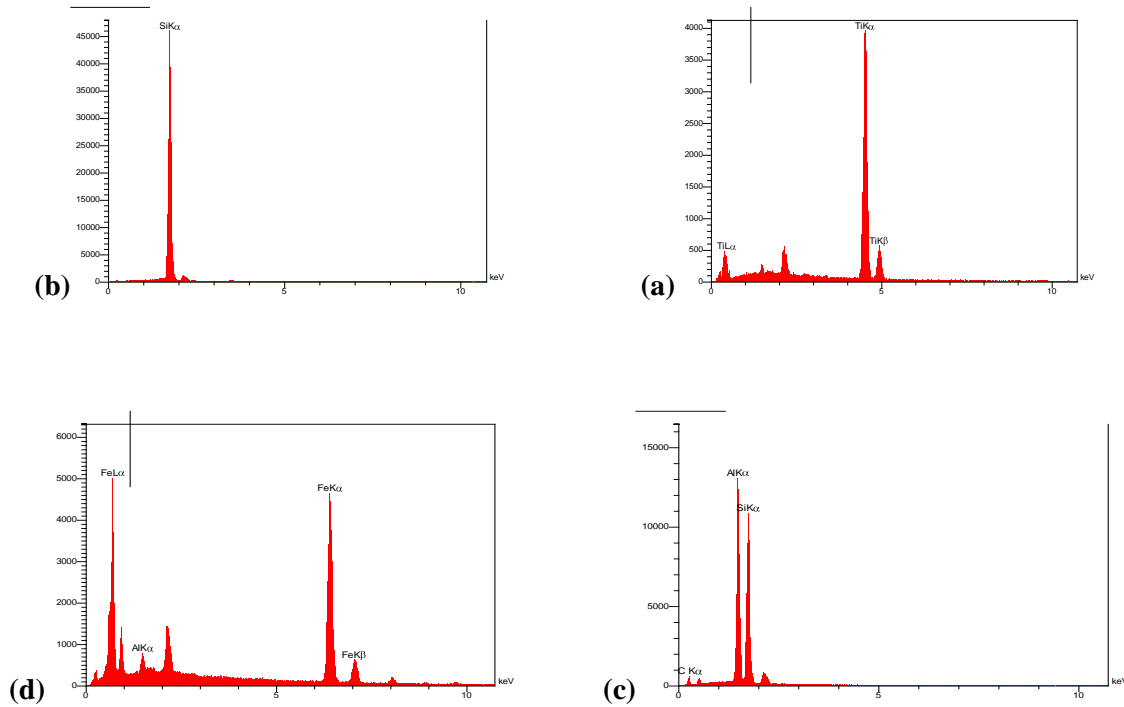
Figure 2. EDXA analysis for A, B, C, and D points in Figure 1(b).

Based on the maximum peaks, it is seemed that the particles A, B, C, and D in the precursor are TiH_2, Si, SiC, and Fe, respectively. Fig. 3 illustrates relative densities, and images of the cellular structure for AlSi7SiC3, AlSi7SiC3Fe1, and AlSi7SiC3Fe3 composite foams, which took out from the thin-walled tubes (mould) after foaming and cutting in longitude section direction versus samples codes. The relative densities of samples with CMF-22-0, CMF-22-1, and CMF-22-3 codes are 0.38, 0.35, and 0.31, respectively.

It can be seen that all the produced foams present a roughly closed-cell structure and the magnitude of pores per inch (PPI) at the cross-section of the foams was between 25-32 PPI. However, the composite foam without Fe have approximately non-uniform distribution and cell size, in comparison to the composite foams containing Fe. It is obvious from the cellular structure of the composite foams without Fe that there are significant variations in closed-cells size and cells wall thickness. In fact, there are several dispersed big voids with coarse surface in cross-section of the foams without Fe. In addition, defects such as drainage, big void, and crack are observed for the foams without Fe composite.

As it is illustrated in Fig. 3, it can be noted that as the Fe powder increases, the cell size increase as well. However, by adding Fe powder into the AlSi7SiC3 composite foam, the association with the SiC particles increases the viscosity (due to their high melting point) and thus reduces the flow-ability of molten melt, which should lead to the thickening of the cells wall. The presence of SiC particles so helps the retention of molten melt and the flow of it is hindered in all directions (the Gibbs–Marangoni effect), whereas Fe with formation of Fe-Si-Al intermetallic compounds can increase the surface tension and the capillarity.

Sample Code	Relative density	Image	Sample Code	Relative density	Image	Sample Code	Relative density	Image
CMF-16-0	0.42		CMF-16-1	0.36		MF-16-3	0.39	
CMF-22-0	0.38		CMF-22-1	0.35		CMF-22-3	0.31	
CMF-32-0	0.34		CMF-35-1	0.32		CMF-35-3	0.30	

Fig.3 Longitude section of the AlSi7SiC3Fe(Y) foams versus their codes and relative densities.

In this case, foam cell walls can be thinner during growth bubbles without cell coalesces and bursting bubbles. Thus, the presence of Fe powder helps in providing better stability, where the cells grow to larger sizes without collapsing or rupturing. It is seemed that samples with 1%wt. Fe have better cellular structure, especially, for the CMF-22-1 sample. As Fig.4, indicates, AlSi7SiC3Fe3 composite foams have thinner walls (images A(3), which obtained from cross the row: A and the column: (3), in Fig.4) distorted and jagged wall (image E(3)) in comparison with AlSi7SiC3Fe1, and AlSi7SiC3 composite foams.

Therefore, it can be deduced that when the Fe powder increases, the cell size increase as well. However, the size of SiC particles and the thickness of the cells walls are decreased. For examples in magnification of more than X4000, the spread SiC particles in the inner surface of cells, as shown in Fig.4, images E(1), E(2), and E(3), they have been finer by increasing of wt. %Fe, respectively. According to Table 2 and ternary phase diagram at Fig.5, It seems that Al-Si-Fe intermetallic compounds can be the reason of foams substructure variations (size, thickness and morphology) in Fig.4.

3wt.%Fe	1 wt.% Fe	0 wt.% Fe
(3)	(2)	(1)

A

X80   X250   X125

E

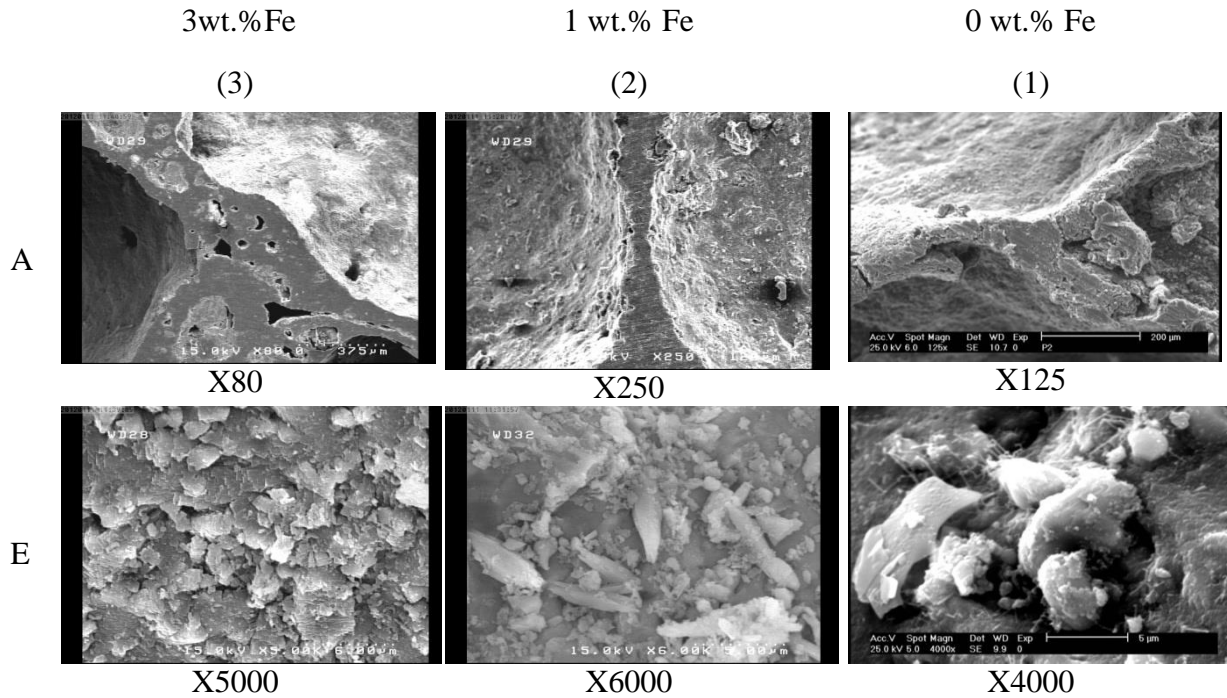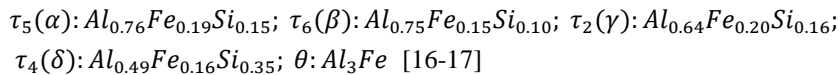X5000   X6000   X4000

Fig.4. Substructures of closed cell foam versus wt. % Fe (columns: (1), (2), and (3)) and magnification (rows: A and E).

Table 2. Reactions and thermodynamic data in the Al-rich corner of the Al-Si-Fe system
(see phase diagram of Fig.5)

Reaction-point	Reaction	Temp (oC)	Reaction-line	Reaction	Temp.range (oC)
P1	$l + \theta + \gamma \to \alpha$	766	P1-U1	$l \to \gamma + \alpha$	648-751
P2	$l + \gamma + \delta \to \beta$	665	P1-U2	$l \to \theta + \alpha$	636-766
U1	$l + \gamma \to \alpha + \beta$	648	P2-U1	$l \to \gamma + \beta$	648-665
U2	$l + \theta \to \alpha + (Al)$	636	P2-U4	$l \to \delta + \beta$	596-665
U3	$l + \alpha \to \beta + (Al)$	609	U1-U3	$l \to \alpha + \beta$	609-648
U4	$l + \delta \to (Si) + \beta$	596	U2-U3	$l \to (Al) + \alpha$	609-636
E1	$l \to (Al) + (Si) + \beta$	576	U3-E1	$l \to (Al) + \beta$	576-609
-	-	-	U4-E1	$l \to (Si) + \beta$	576-596

$\tau_5(\alpha): Al_{0.76}Fe_{0.19}Si_{0.15}$; $\tau_6(\beta): Al_{0.75}Fe_{0.15}Si_{0.10}$; $\tau_2(\gamma): Al_{0.64}Fe_{0.20}Si_{0.16}$;

$\tau_4(\delta): Al_{0.49}Fe_{0.16}Si_{0.35}$; $\theta: Al_3Fe$ [16-17]

One of the possible reasons could be as follow. It is noticeable that in the AlSi7SiC3Fe3 composite foams, there are some micro-porosities in the plateau region of cells, as shown in Fig.4, image A(3). On the other hand, the Fe and Si are soluble in liquid Al but they have very little solubility in the solid, which is shown in Fig.5 in a blue line. Fe tends to combine with other elements to form intermetallic compounds

during transforming from the liquid's temperature to the solids temperature (thermal path P1→U2→(Al)→E1 on Fig.5). In the absence of Si, the dominant intermetallic phases that forms are Al_3Fe (θ-phase) and Al_6Fe [16]. However, when Si is presented, the dominant phases are Al_8Fe_2Si (α-phase), Al_5FeSi (β-phase), Al_3FeSi (γ-phase), and Al_4FeSi_2 (δ-phase) based on the corner of Al-Si-Fe phase diagram in Fig.5 [16-18].
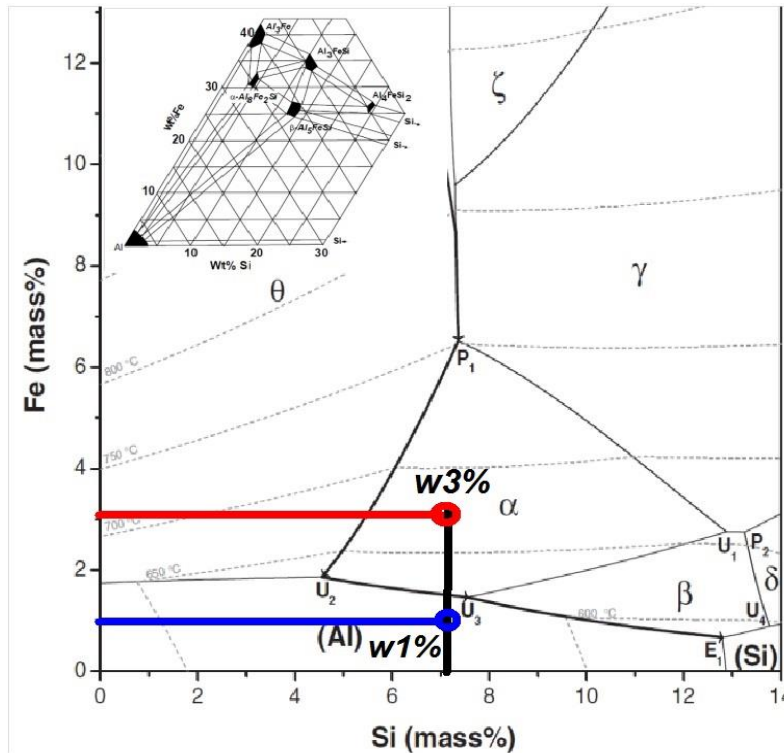

Fig.5. Corner of Al-Si-Fe ternary phase diagram and stable intermetallic compounds.

In this case that Fe is 3%wt temperature, liquids are shown in Fig.5 in a red line, and thermal path will be fromed (P1→α→β→U1→P2→U4) at slow cooling rate. Some of the Fe intermetallic compounds mentioned above are quite obvious within the microstructures of Al-Si alloys, and can usually be distinguished under the microscope with their morphology and color. For example, the α-phase forms in a script-like morphology and β-phase has a needles or flake form [18-19]. It is revealed that the morphologies of Fe inter-metallic phases are responsible for the foam cellular structure and the mechanical properties [18-20]. It is reported that cooling rate of Al foams liquid containing of Fe and Si, have significant effect on the morphology and the type of both the Al8Fe2Si(α) and the Al5FeSi (β) inter-metallic [16-17, 21]. Although during the foaming process through powder metallurgy route, the foaming time often is less than 10 minutes, the Fe and Si powders can be solved in the liquid Al alloys as partially, dependent on the time and temperature of foaming treatment. The substructures of AlSi7SiC3Fe3 composite foams are shown in Fig. 6. The substructure of the composite foams depicts that the inter-metallic phases (marked "P0") are reasonably non- uniform distribution and irregular in shape. Microphotograph of the cell wall at higher magnification is also depicted in Fig. 6, (marked P1), which

exhibits fair bonding between the inter-metallic phases and the matrix alloy, as far as any discontinuity is not observed at the interface. Although during the foaming process, the gas is released and may accumulate at the interface of the inter-metallic phase and the matrix, the microstructure reveals a semi-strong interface, which is continuously distributed without micro-porosity, crack and gap at the inter-metallic and matrix interface. Therefore, the micro-bubbles should move to the plateau region, due to the viscosity and capillarity effects. Fig.4, image A(3) shows the object that is in agreement with reference [22]. Fig. 6 (marked P1) shows the location and compound of the inter-metallic phase in the cell structure and illustrates that inter-metallic phases tend to extend into the gas bubble.
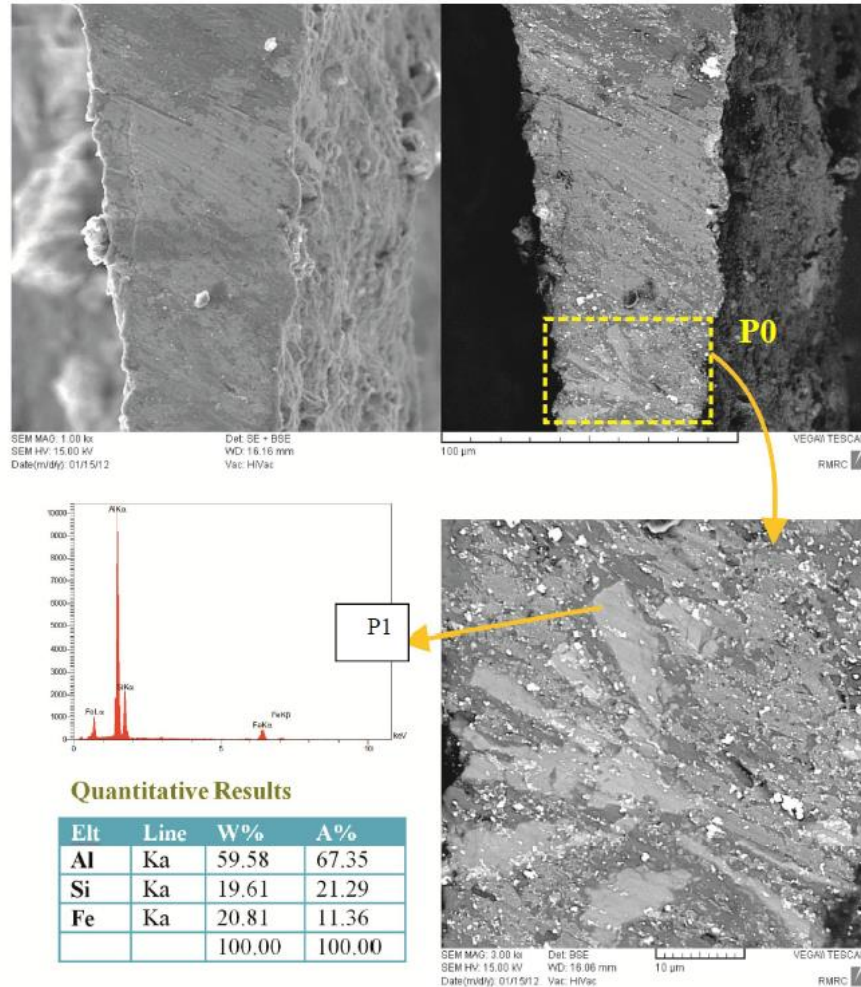

Quantitative Results

Elt	Line	W%	A%
Al	Ka	59.58	67.35
Si	Ka	19.61	21.29
Fe	Ka	20.81	11.36
		100.00	100.00

Fig.6.Intermatallic Al-Si-Fe and EDXA results within cell wall thickness AlSi7SiC3Fe3 foam.

The AlSi7SiC3Fe3 foam EDXA results at interface of the inter-metallic compounds and the matrix alloy (marked "P1") which is presented in Fig.6. It can be observed that Al, Fe, and Si elements have 67.25, 21.29, and 11.36 atomic percent (Al:Si:Fe = 5.9:1.8:1), respectively. Therefore, the compound form of the inter-metallic phase can be one of the Al8Fe2Si (α-phase), Al5FeSi (β-phase), and Al4FeSi2 (δ –phase) [23]. Thus with the increasing of cooling rate at the final stages of solidification, Fe δ -platelets precipitate in the cell wall [24]. Also Al4Fe2Si (δ -phase) based on the results of EDXA and its flack or

platelet shape is among the favored compound, which is in line with results of references [16-17]. Finally, it is concluded that during the foaming process, the increasing of Fe in the AlSi7SiC3Fe composite foams lead to the increase size of the cell and decrease the thickness of the cells walls. In addition, during solidification of the liquid foams, Al4Fe2Si- δ –platelets was formed with the strong bond. The δ – platelets tend to extend into the gas bubble and precipitate in the cell wall (due to distortion of cell walls), whereas micro-porosities dispose toward accumulation at plateau regions of cells. Both of them (the inter-metallic compound and the micro-porosities) have the roles of stress concentration zones, and they can significantly affected mechanical and physical properties of the foams such as compression test.

3.2. Compression response for metal foams

Fig. 7 shows the effect of Fe wt. % on stress-strain curves for the three composite metal foams during the compression test.
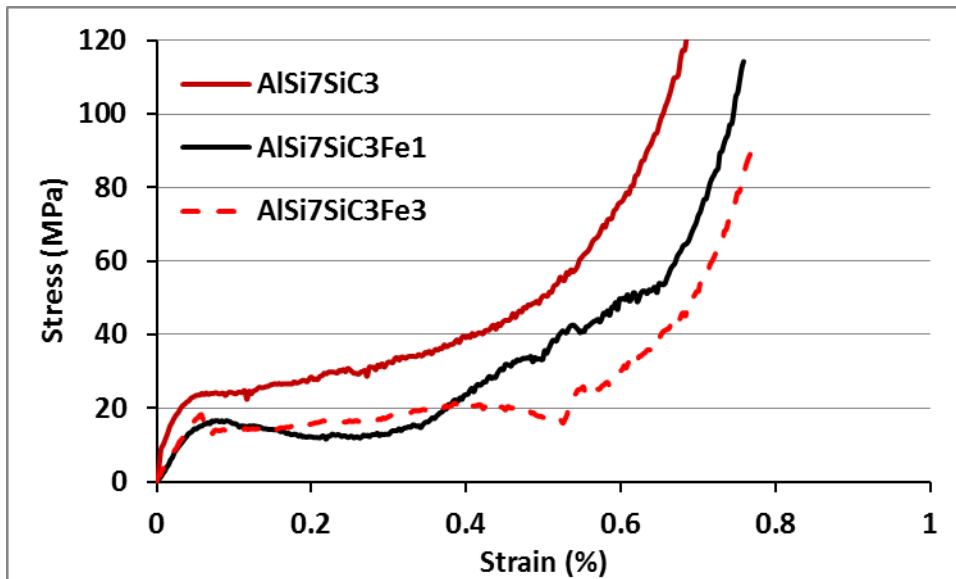

Fig.7. Stress-strain curves of the three composite metal foams, during uniaxial and quasi static plastic deformation.

Alike other Al composite metal foam, they have characteristic of compressive stress–strain curves, which involve three distinct stages [2, 4, 25]. At elastic strain, the stress increases linearly with increasing strain in elastic deformation region meaning that the foam cell walls bend as elastic buckling. Then a long plateau of plastic deformation occurs at approximately smooth stress, and foam bubble walls buckle as plastic and the cells are softly crushed or crashed. After the densification strain (0.5-0.6% strain in Fig.7) it is shown that the stress abruptly increased, since the foam cell walls collapsed and contacted together. Fig. 7 also indicated that the AlSi7SiC3 (without Fe) composite foam have the maximum slope variety of the stress-strain curves through the plateau plastic deformation region, whereas for the AlSiSiC3Fe foams, the slope with the increasing of Fe element unexpectedly reduced (the dotted-curves, in Fig.7). As it was seen, it can be deduced that the presence of Fe element in the Al composite foam does not significantly affect the compression stress–strain response at the elastic region. However, the addition of Fe has a considerable impact on the plateau plastic deformation region, especially in case of strain-

hardening phenomenon and toughness. It seems that brittleness of AlSi7SiC3Fe-(Y) foams is due to the dispersion of the intermetallic compounds within the foam cell walls and the accumulation of micro-voids within the plateau zones, in comparison with the AlSi7SiC3 samples.

The ductile behavior of foam samples containing Fe might be attributed to the relatively more brittleness in comparison to the AlSi7SiC3 foams. Therefore, the behavior of strain-hardening exponent for all samples, during plateau plastic deformation, can be noted. The flow stress of a material is generally expressed as a function of plastic strain through $\sigma = K\varepsilon^n$ equation, where "n" is the strain-hardening exponent, and "K" is the plastic strength coefficient. The variation of $\ln(\sigma)$ with $\ln(\varepsilon)$ for all of the composite foam at plastic deformation regions (Not elastic) are shown in Fig. 8. Moreover, the two mechanisms and their governing equations can be noted for each material in Fig. 8.
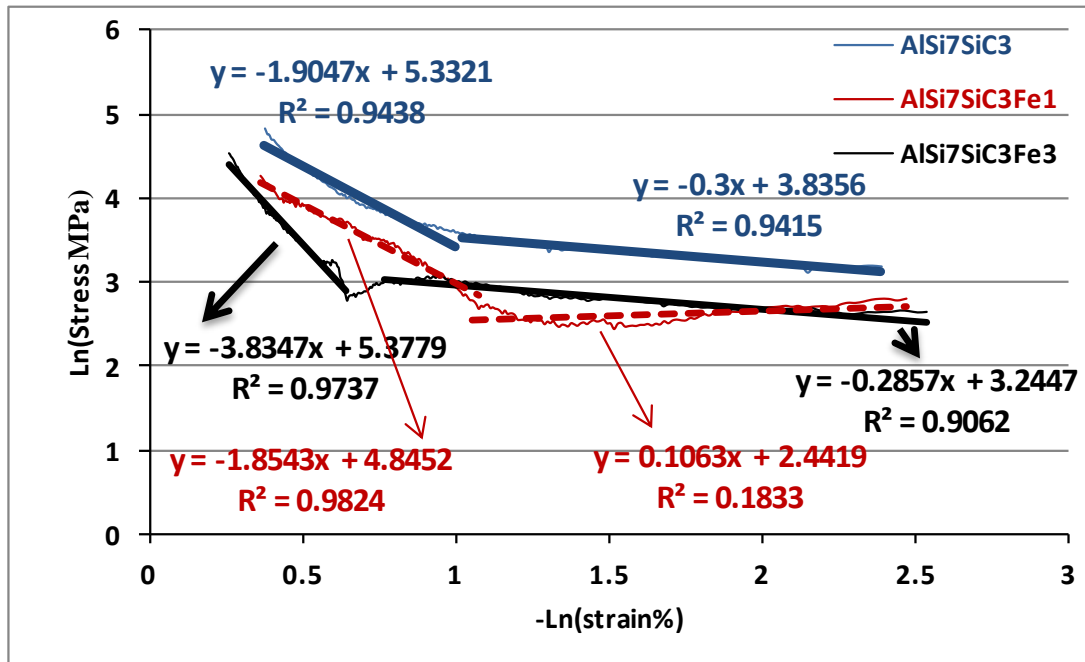

Fig.8. Plot of Ln(σ) versus Ln(ε) for the three foams during plastic deformation in Fig.7.

The first mechanism has a strain-hardening exponent for lower strains with slope "$n1$" (before densification strain or soft plastic deformation) and other mechanism has a higher strain-hardening exponent with slpoe "$n2$" (after densification strain or hard plastic deformation). The strain-hardening exponents and the plastic strength coefficients of the investigated foams are given in Table 3. It can be observed that the addition of Fe element significantly affects the strain-hardening exponents of all composite foams. The strain-hardening exponent of the AlSi7SiC3Fe foams is lower than that of AlSi7SiC3 foam. However, by increasing the Fe powder from 1 to 3wt. %, an increase in the strain-hardening exponent of the AlSi7SiC3-(Fe) composite foams occurs.

Table 3. Determination of "n" and "k" coefficients of hardening-strain equation for all the samples in Fig.8

sample code	Eq(n1)	Eq(n2)	/ n1	/ n2	ln(k1)	ln(k2)	Line-line intersection	
							ln(ε)	ln (σ)
CMF-20-0	Lnσ =1.9047Lnε + 5.3321	Lnσ =0.3Lnε +3.8356	1.91	0.30	5.33	3.83	1	3.5
CMF-20-1	Lnσ =1.8543Lnε + 4.8452	Lnσ =-0.1063Lnε +2.442	1.85	-0.1	4.84	2.44	1.11	2.7
CMF-20-3	Lnσ=3.8347Lnε + 5.3779	Lnσ=0.2857Lnε +3.2447	3.83	0.28	5.38	3.25	0.7	2.7

3.3. Effect of Fe on energy absorption capacity

Fig. 9 illustrates the effect of Fe additive on the energy absorption capacity at a fixed strain rate.
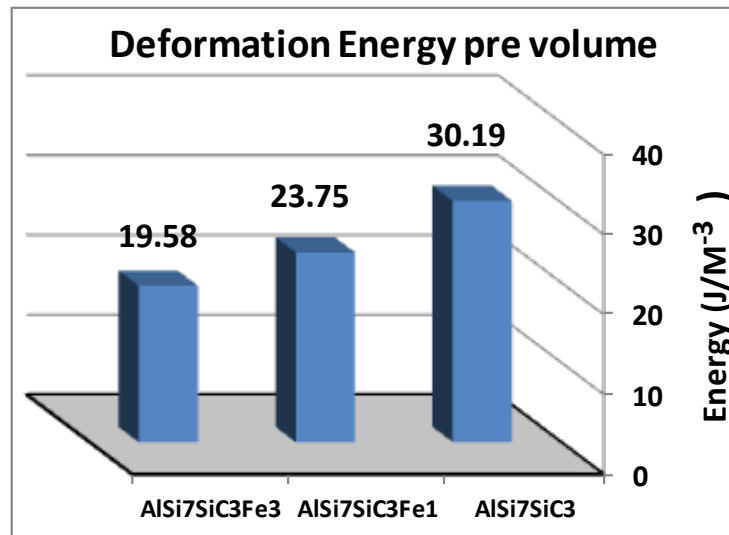

Fig.9. Obtained absorption energy from curves in Fig.7 during the plastic deformation of foams under uniaxial loading.

In Fig.9, the absorbed energy during the deformation plastic of composite foams is shown where W, was calculated from Equation (1):

$$W = \int_{\varepsilon_0}^{\varepsilon_d} \sigma(\varepsilon). d\varepsilon \tag{1}$$

Where the upper limit of integration (ε_d) is determined from cross-cut lines in Fig.8, and the data of Table 3.

In Fig. 9, the absorbed energies of the composite foams are plotted as a function of wt. % Fe. The composite foams show the decreasing energy absorption for foams with increasing of wt.% Fe. It can be noted from Fig.9, energy absorption of the AlSi7SiC3 foams is more than both the AlSi7SiC3Fe1 and the AlSi7SiC3Fe3 foam This is can be attributed to 2 reasons: i) the higher yield and plateau stress of the AlSi7SiC3 in Fig.7, and ii) there is not the breaking or the oscillation during strain-hardening in the AlSi7SiC3 foams. It seems that adding of Fe decrease the absorption energy due to presence of the intermetallic compounds (*see subsection3.1*) of Fe within the walls of foam bubbles (see Fig. 4, and

Fig.6). Therefore, for the AlSi7SiC3Fe-(Y) composite foams, which their cell wall containing (α+β) for wt. % Fe < 2 or (α+δ) for wt. % Fe > 2 (according to thermal paths on Fig.5 and Table 2), dependent on low and high cooling rate, respectively, an additional energy is absorbed at ASi7SiC3:Fe1 samples due to the presence of the concentration of stress around of the intermetallic within the cell wall (see Fig.4, and 6),as like stress intensity around of the micro-void within cell plateau region (see image A(3) in Fig.4). On the basis of the above results, it can be deduced that foams containing of Fe, the solid bubbles (with Fe-Intermetallic compounds) have a good plastic buckling, and if they have been surrounded with some micro-voids, due to suitable distribution of plastic hinge points at the walls and plateau regions, they show a wide range of the strain at a stress level approximately smooth. This behavior is more suitable for energy absorbers at the time of crash impact. Therefore the addition of Fe to the AlSi7SiC3 foam, during compression test until the densification strain, can decrease positive-slope of strain-hardening toward a smooth slop (nearly zero slop), only for foams with Fe <2 wt.% which Fe is as (α+β) intermetallic compound. However for the foams with wt. % Fe>2 wt.% and as (α+δ) intermetallic compound, the stress level during the densification strain will not be smooth.

4. Conclusions

1. Cellular structure and Micro-structure of composite foams have a significant role on the behavior of plastic deformation of the AlSi7SiC3foams and AlSi7SiC3Fe foams. In cases that foam cells walls can be thinner during the growth bubbles without the cells coalesce the absorption energy will be increased by decreasing the foams relative density.

2. During AlSi7SiC3Fe foaming processes by powder metallurgy route, some intermetallic such as α+β and α+δ are formed depending on the cooling rate and the percent of Fe element, which strongly affected on mechanical and physical properties. Results showed α+δ formed at high cooling rate and Fe percent of more than 2 wt. %, and α+β formed at lower cooling rate and Fe percent less than 2 wt. %.

3. During foaming process, the micro-voids are accumulated within the cell plateau region (see Fig.4) and the flack Fe-intermetallic compounds are moved to the cell thin walls as a perpendicular (see Fig.6), and thus both of them act as the stress concentration pointes.

4. Fe additive in the AlSi7SiC3 composite foams affected on the hardening-strain exponent. In case 1wt. %Fe the hardening-strain exponent "n2" is near to zero that is related to the foam with 3wt. %Fe. It is clear that "n2≈0" referred to the plastic deformation without work-hardening. In this condition, the plateau stress versus strain is alike a horizontal line. Therefore, the AlSi7SiC3Fe1 rather than the AlSi7SiC3Fe3 is due to the hardening-strain exponent that is near to zero and the higher energy absorption (approximately 21%) of the AlSi7SiC3Fe1.

5. References

[1] J. Baumeister, J. Banhart, M.Weber, Aluminum foams for transport industry, *Materials & & Design*, 18(4/6), (1997) 217-220.

[2] T. Mukai, T. Miyoshi, S. Nakano, H. Somekawa, K. Higashi, Compressive response of a closed-cell Aluminum foam at high strain rate, *Scripta Materialia,* 54 (2006) 533–537.

[3] D. Lehmhus, J. Banhart, M.A. Rodriguez-Perez, Adaptation of Aluminum foam properties by means of precipitation hardening*, Materials Science and Technology,* 18 (2002) 1–6.

[4] A.G. Evans M.F. Ashby, N.A. Fleck, L.J. Gibson, J.W. Hutchinson, H.N.G. Wadley, *Metal foams: A design guide*, Elsevier, UK, (2000), chapter: 11.

[5] M. F. Ashby L. J. Gibson, *Cellular Solids: Structure and Properties.* Solid State Science., UK: Cambridge, (1997), chapter:4.

[6] W. abramowicz and T. Wierzbicki, Axial crushing of foam-filled columns, Journal *of. Mechanical Science*, *30*, Issues *3-4* (1988) 263-271.

[7] M. Langseth, A.G. Hanssen, and O.S. Hopperstad, Optimum design for energy absorption of square Aluminum columns with Aluminum foam filler, I*nternational Journal of Mechanical Sciences*, 43 (2001)153-176.

[8] A.F. Bastawros, H. Bart-Smith, and A.G. Evans, Experimental analysis of deformation mechanisms in a closed-cell aluminum alloy foam. *Journal of the Mechanics and Physics of Solids*, 48 (2000) 301-322.

[9] A.K. Toksoy and M. Guden, Partial A: Foam filling of commercial 1050H14 crash boxes: the effect box column thickness and foam relative density on energy absorption, *Thin-walled structures,* 48(2010) 482-494.

[10] W. Yan, E. Durif, Y. Yamada and C. Wen, Crushing Simulation of Foam-Filled Aluminum Tubes, *Materials Transactions*, 48, No. 7 (2007) 1901-1906.

[11] W. Deqing and S. Ziyuan, Effect of ceramic particles on cell size and wall thickness of aluminum foam, *Materials Science and Engineering A*, 361 (2003) 45–49.

[12] P. Mondal, M.D. Goel, and S. Das, Effect of strain rate and relative density on aluminum-fly ash composite foam, *Materials & Design* 30 (2008) 1268–1274.

[13] M.J. Khajeali, Compressive response of the composite metallic foam filled-tubes and effective parameters, *M.Sc. Thesis, Amirkabir University*, (2011).

[14] A. Daoud, ,Compressive response and energy absorption of foamed A359–Al_2O_3 particle composites, *Journal of Alloys and Compounds,* 486 (2009) 597–605.

[15] Y. Luo, S. Yu,W. Li, J. Liu, and M. Wei, Compressive behavior of SiCp/AlSi9Mg composite foams, *Journal of Alloys and Compounds* 460 (2008)294–298.

[16] S. Lee, B. Kim and S. Lee, Prediction of Solidification Paths in Al-Si-Fe Ternary System and Experimental Verification: Part I. Fe-Containing Hypoeutectic Al-Si Alloys, *Materials Transactions*, Vol. 52, No. 5 (2011) 1053-1062.

[17]. Sanghwan Lee, Bonghwan Kim and Sangmok Lee, Prediction of Solidification Paths in Al-Si-Fe Ternary System and Experimental Verification: Part II. Fe-Containing Eutectic Al-Si Alloys, *Materials Transactions,* 52, No. 6 (2011)1308-1315.

[18] E. Amsterdam, P. R. Onck, and J. TH. M. Dehosson, Fracture and microstructure of open cell Aluminum foam, *Journal of Materials Science,* 40 (2005) 5813–5819

[19] G. Mrówka-Nowotnik, J. Sieniawski, and M. Wierzbiñska, Intermetallic phase particles in 6082 aluminum alloy, *Archives of Materials Science and Engineering*, 28, Issue 2 (2007) 69-76.

[20] E. Amsterdam, N. Babcsán, Jeff T.M. De Hosson, P.R. Onck, and J. Banhart, Fracture behavior of metal foams made of recycled MMC by the melt route, *Materials Transactions*, 47(6) (2006) 2219-2222.

[21] L. Sweet, S.M. Zhu, S.X. Gao, J.A. Taylor, and M,A. Easton, The effect of iron content on the Iron-containing intermetallic phases in a cast 6060 Aluminum alloy, *Metallurgical and materials transaction* A, 42A (2011)1737-17-49.

[22] A.R. Kennedy, S. Asavavisitchai, Effects of TiB2 Particle Addition on the Properties of PM Al Foams, *Scripta Materialia* 50 (2004) 115–119.

[23] Anton Gorny, Characterization of Major Intermetallic Phases in solidified Al-xSi-yFe-zSr alloy, *Ph.D. thesis (open accesses), McMaster University*, (2012).

[24] M. Timpel, N. Wanderka , R. Grothausmann , and J. Banhar , Distribution of Fe-rich phases in eutectic grains of Sr-modified Al-10wt%Si-0.1wt% Fe casting alloy,
Journal of Alloys and Compounds, 558 (2013) 18–25.

[25] J. Banhart, Manufacture, characterization and application of cellular metals and metal foam, *Progress in Materials Science*, 46 (2001) 559–632.